# Dependence of Photocatalytic Activity on Aspect Ratio of Shape-Controlled Rutile Titanium(IV) Oxide Nanorods

# Dependence of photocatalytic activity on aspect ratio of shape-controlled rutile titanium(IV) oxide nanorods

*Naoya Murakami, Satoshi Katayama, Misa Nakamura, Toshiki Tsubota and Teruhisa Ohno**

Department of Applied Chemistry, Faculty of Engineering, Kyushu Institute of Technology, 1-1 Sensuicho, Tobata, Kitakyushu 804-8550, Japan

AUTHOR EMAIL ADRESS: murakami@che.kyutech.ac.jp

* CORRESPONDING AUTHOR: Teruhisa Ohno

TEL & FAX: +81-93-884-3318, EMAIL ADRESS: tohno@che.kyutech.ac.jp

**ABSTRACT**

Shape-controlled rutile titanium(IV) oxide ($TiO_2$) nanorods with various aspect ratios were prepared by two-step synthesis in the presence of two kinds of inorganic anions. The first synthesis step from titanium(III) chloride solution induced the formation of aggregated needle-like rutile $TiO_2$, the shape of which largely depended on the inorganic anion used. Moreover, shape-controlled rutile $TiO_2$ rods with {110} side crystal faces and {111} and/or {001} edge crystal faces were obtained by hydrothermal treatment of the needle-like rutile $TiO_2$. Their aspect ratios were largely influenced by the starting material used in the hydrothermal treatment. The photocatalytic activity for decomposition of acetaldehyde increased with decreasing aspect ratio because the surface area ratio of {111} and/or {001}

to {110} exposed crystal faces, which are attributed to oxidation and reduction sites respectively, became more optimal.

**KEYWORDS**

Photocatalyst, titanium(IV) oxide, rutile rod, separation of redox sites.

**MANUSCRIPT TEXT**

## 1. Introduction

Photocatalytic reactions over semiconductor particles have been utilized in various applications, including environmental remediation,[1,2] water splitting,[3–5] and reductive conversion of carbon dioxide.[6] The photocatalytic activity over semiconductor particles is thought to depend on their physical and chemical properties, such as their crystal structure, specific surface area, particle size, and defect density.[7] Therefore, optimizing these properties has been the conventional strategy for enhancing photocatalytic activity, though the most suitable property to optimize for a specific reaction differs depending on the reaction substrate.

Since the report on titanium(IV) oxide ($TiO_2$) with specific exposed crystal faces by Ohno et al. in 2002,[8] various other groups have reported $TiO_2$ with a similar surface structure.[9–23] Our group has synthesized shape-controlled anatase and rutile $TiO_2$ whose photocatalytic properties depend on the specific exposed crystal faces due to preferential reduction and oxidation.[24–27] Although the mechanism for photocatalytic reactions over $TiO_2$ with specific exposed crystal faces is still under discussion, these results imply that the exposed crystal face is an important factor that affects photocatalytic reactions. This is reasonable since the surface energy, the chemical surface state, and the number and energy state of defective sites predominantly depend on the atomic arrangement of exposed crystal faces.[28–30] The effect of these surface properties on photocatalytic reactions will be enhanced with increasing surface-to-bulk ratio (i.e., decreasing particle size) because photocatalytic reactions mainly occur in interfacial regions.

Decahedral anatase with {101} and {001} exposed crystal faces[8,9,12,14–18,27] and dodecahedral rutile with {110} and {101},[8] or {110} and {111} exposed crystal faces[10,11,24] have been synthesized as well-defined $TiO_2$ particles. To form these exposed crystal faces requires using inorganic or organic compounds as shape-control reagents,[10–12,15,24,27] specific precursors[13,17,18] and specific preparation conditions.[16] The influence of inorganic anion on the nucleation of $TiO_2$ has been well studied. Chloride ($Cl^-$) and sulfate ($SO_4^{2-}$) anions are reported to influence the formation of rod-like rutile, octahedral anatase, and decahedral anatase, respectively.[10–12,19] Since Yang et al. synthesized decahedral anatase with a high percentage of {001} faces,[20] anatase prepared by hydrothermal treatment involving fluoride ($F^-$) ions has been intensively investigated.[14,21,22] The photocatalytic activity depends on the surface area ratio of {001} to {101} faces of decahedral anatase,[14,23,27] which implies that controlling the surface structure (specifically, the kinds of exposed crystal faces and their ratios) can be used to control the reaction properties.

Ohno et al. have reported shape controlled rutile rod and its photocatalytic activity depended on their surface structure, which could be controlled by using shape-control reagents or chemical etching.[25] These rutile rods predominantly have {110} and {111} exposed crystal faces, which were respectively attributed to reduction and oxidation sites.[24] The rutile rods had aspect ratios of over five due to preferential growth along the [001] direction, indicating that they had a large {110} surface area and a small {111} surface area. A surface structure with a larger surface area of reduction sites than oxidation sites may be desirable for pristine rutile $TiO_2$ because the bottleneck reaction for conventional organic decomposition under aerated conditions is oxygen reduction rather than oxidation because of the conduction and valence band potentials of rutile $TiO_2$. This tendency is possibly more pronounced for rutile than anatase since the conduction band of rutile is less negative than that of anatase. Furthermore, one plausible reason for relatively high photocatalytic activity of the rutile may be because multi-electron reduction of oxygen occurs as a result of separation of redox sites which was induced by

specific exposed crystal faces. However, it should be possible to further enhance photocatalytic reactions by optimizing the aspect ratio of the rods (Scheme 1).

In the present study, we prepared shape-controlled rutile $TiO_2$ rods with various aspect ratios by a two-step synthesis involving hydrolysis and hydrothermal processes in the presence of a shape-control agent (sodium chloride (NaCl) and/or sodium perchlorate ($NaClO_4$)). The surface structure and specific surface area of the rods were analyzed as functions of the aspect ratio of shape-controlled rutile rods, and the dependence of the photocatalytic activity of acetaldehyde decomposition on the aspect ratio was examined.

## 2. Experimental

### 2.1. Sample preparation

#### 2.1.1. First-step growth at room temperature

Aqueous titanium(III) chloride ($TiCl_3$) solution (50 $dm^3$, 0.15 mol $dm^{-3}$) containing 0, 0.5, and 3.0 mol $dm^{-3}$ of NaCl and/or $NaClO_4$ in a beaker was stirred at room temperature for one week. The residue was washed several times with Milli-Q water until the ionic conductivity was <10 μS $cm^{-1}$. The particles were dried at 80 °C for 12 h. Samples were prepared with and without additives ($NaClO_4$ and NaCl); these samples are denoted by S(Cl-n,$ClO_4$-m), where n and m indicate the concentration (mol $dm^{-3}$) of chloride and perchlorate ion in solution.

#### 2.1.2. Second-step growth under hydrothermal conditions

A suspension of the prepared $TiO_2$ in section 2.1.1 (50 $dm^3$) in a Teflon bottle was ultrasonically agitated and the bottle was then sealed with a stainless-steel jacket and heated at 200 °C for 24 h in an oven. After this hydrothermal treatment, the residue was washed several times with Milli-Q water until the ionic conductivity was <10 μS $cm^{-1}$. The particles were dried at 80 °C for 12 h. The samples prepared by hydrothermal treatment of S(Cl-n,$ClO_4$-m) are denoted by HS(Cl-n,$ClO_4$-m).

2.1.3. Second-step growth under hydrothermal conditions with $NaClO_4$

The $TiO_2$ prepared with NaCl in section 2.1.1 was treated under the same hydrothermal conditions in the presence of $NaClO_4$, and $TiO_2$ was obtained by the same post treatment. The obtained samples prepared by hydrothermal treatment of S(Cl-n,$ClO_4$-0) are denoted by H($ClO_4$-m)S(Cl-n,$ClO_4$-0), where m indicates the $NaClO_4$ concentration (mol $dm^{-3}$) of the solution.

2.1.4. One-step hydrothermal condition with additives

As reference samples, $TiO_2$ was prepared by one-step hydrothermal treatment. Aqueous $TiCl_3$ solution (50 $dm^3$; 0.15 mol $dm^{-3}$) containing 1.0 mol $dm^{-3}$ of NaCl or 0.5 mol $dm^{-3}$ of $NaClO_4$ was treated under the same hydrothermal conditions, and $TiO_2$ was obtained by the same post treatment. The samples prepared by one-step hydrothermal treatment with 1.0 mol $dm^{-3}$ of NaCl and 0.5 mol $dm^{-3}$ of $NaClO_4$ are denoted by OH(Cl-1) and OH($ClO_4$-0.5).

2.2. Characterization

The crystal structures of the $TiO_2$ powders were characterized by X-ray diffraction (XRD; Rigaku, MiniFlex II) with Cu Kα radiation (λ = 1.5405 Å). The specific surface areas ($S_{BET}$) of the particles were determined using a surface area analyzer (Quantachrome, Nova 4200e) using the Brunauer–Emmett–Teller equation. The morphology of prepared $TiO_2$ particles was observed by transmission electron microscopy (TEM; Hitachi, H-9000NAR). Longer average lengths ($L_{ave}$) and shorter average widths ($W_{ave}$) were estimated by TEM observation on more than 80 particles ($\sigma_L$ and $\sigma_W$ are the standard deviations of $L_{ave}$ and $W_{ave}$, respectively), and the aspect ratio ($r_{asp}$) is defined as $r_{asp} = L_{ave}/W_{ave}$.

2.3. Photocatalytic evaluation

The photocatalytic activities of the $TiO_2$ samples were evaluated by photocatalytic decomposition of acetaldehyde. One hundred milligrams of $TiO_2$ powder, which completely extinguished the incident radiation, was spread on a glass dish (5.6 $cm^2$) and the glass dish was placed in a 125-$cm^3$ Tedlar bag (As One). Five hundred parts per million of gaseous acetaldehyde was injected into the Tedlar bag and photoirradiation was performed at room temperature after the acetaldehyde had reached adsorption equilibrium. The gaseous composition in the Tedlar bag was 79% of $N_2$, 21% of $O_2$, <0.1 ppm of $CO_2$, and 500 ppm of acetaldehyde and the relative humidity was ca. 30%. A light emitting diode (Nichia, NCCU033) which emitted light at a wavelength of ca. 365 nm was used as the light source. Its light intensity (irradiance) at the photocatalyst surface of 1.0 mW $cm^{-2}$, which was measured with power meter (Ophir, Orion TH) equipped with thermal power sensor (Ophir, 3A-SH). The acetaldehyde and carbon dioxide ($CO_2$) concentrations were estimated by gas chromatography (Shimadzu, GC-8A, FID detector) with a PEG-20 M 20% Celite 545 packed glass column and by gas chromatography (Shimadzu, GC-9A, FID detector) with a TCP 20% Uniport R packed column and a methanizer (GL Sciences, MT-221), respectively.

## 3. Results and discussion

### 3.1. Crystal growth during the first step

$TiO_2$ formation from $TiCl_3$ solution was observed after one week of stirring at room temperature. All the XRD peaks of all the S(Cl-n,$ClO_4$-m) samples were assigned to rutile $TiO_2$ alone (Figure S1 in supporting information). Low-intensity, broad peaks indicate that the rutile crystallites are small. Actually, $S_{BET}$ of all the samples was >100 $m^2$ $g^{-1}$, which is relatively high for rutile particles (174, 162, 109, 128, 129, and 276 $m^2$ $g^{-1}$ for S(Cl-0,$ClO_4$-0), S(Cl-0,$ClO_4$-0.5), S(Cl-0,$ClO_4$-3), S(Cl-0.5,$ClO_4$-0), S(Cl-3,$ClO_4$-0.5), and S(Cl-3,$ClO_4$-3), respectively). No large differences were observed between the XRD patterns of S(Cl-0,$ClO_4$-0), S(Cl-0,$ClO_4$-0.5), and S(Cl-0,$ClO_4$-3); however, samples with higher NaCl concentrations had less intense, wider XRD peaks, suggesting that a higher $Cl^-$-ion concentration retards crystal growth.

Figure 1 shows TEM images of samples prepared by stirring in the first synthesis step. All the samples consisted of needle-like $TiO_2$, which was composed of small aggregated crystallites. However, the shape, size, and aggregation state of the samples strongly depended on the kind and concentrations of the additives employed during crystal growth. This result reveals that these differences are a result of using $Cl^-$ and $ClO_4^-$ anions during crystal formation, although the influence of $ClO_4^-$ is relatively small. Using $ClO_4^-$ ions induced radial aggregation of narrower and longer needle-like $TiO_2$, whereas the sample prepared using $Cl^-$ ions exhibited random aggregation of wider and shorter needle-like $TiO_2$. Furthermore, needle-like $TiO_2$ became more aggregated with increasing anion concentration, which is consistent with the observed reduction in $S_{BET}$. S(Cl-3,$ClO_4$-3) showed aggregations of shorter and narrower needle-like $TiO_2$, presumably due to the influences of both $Cl^-$ and $ClO_4^-$.

Several groups have prepared similar rutile needles with urchin-like structures by hydrolysis, hydrothermal, and microwave-assisted hydrothermal processes from $TiCl_3$, titanium(IV) chloride ($TiCl_4$), and titanium(IV) oxychloride ($TiOCl_2$) precursors.[19,31–33] They concluded that using $Cl^-$ ions leads to the formation of rutile $TiO_2$ needles due to a preferred coordinate in the $TiO_6$ unit. In the present study, the change in the needle-like structure (Fig. 1) and the reduction in $S_{BET}$ may be attributed to the effect of both $Cl^-$ and $ClO_4^-$ anions during nucleation. $Cl^-$ has a larger influence than $ClO_4^-$ during hydrolysis because titanium complexes coordinated with $ClO_4^-$ ions are not stable.[34]

3.2. Crystal growth during the second step

XRD patterns of HS(Cl-n,$ClO_4$-m) sample (Figure S2 in supporting information) shows that hydrothermal treatment did not induce formation of a different crystal structure; rather, the peaks attributed to rutile became more intense and sharper. This indicates that hydrothermal treatment induced further crystallization of the rutile phase without producing another crystal phase.

Figure 2 shows TEM images of the samples. They mainly reveal rod-like particles with exposed crystal faces that are attributable to {110} side faces and {111} and/or {001} edge surfaces.[10,11,24] The

rod length primarily depends on the starting material of the hydrothermal treatment. The HS(Cl-0,$ClO_4$-m) samples have relatively long rods. The HS(Cl-0,$ClO_4$-0.5) and HS(Cl-0,$ClO_4$-3) samples had similar rod lengths (Fig. 1b, c), whereas HS(Cl-n,$ClO_4$-0) samples have short rods whose length depends strongly on the $Cl^-$ concentration used in the first step (Fig. 1d, e). These results indicate that the rod length of hydrothermally prepared samples is more dependent on the $Cl^-$ ion concentration than the $ClO_4^-$ concentration during the first step of needle-like $TiO_2$ synthesis. The rods of the HS(Cl-3,$ClO_4$-3) sample were shorter than those of the other samples since the starting material S(Cl-3,$ClO_4$-3) consisted of shorter and narrower needle-like structures than the other starting materials (Fig. 1f).

3.3. Crystal growth with $ClO_4^-$ in the second synthesis step

Similar hydrothermal treatment was performed on the S(Cl-n,$ClO_4$-m) sample in the presence of $ClO_4^-$ anions. The XRD patterns of the H($ClO_4$-m)S(Cl-n,$ClO_4$-0) samples (Figure S3 in supporting information) are similar to those of the HS(Cl-n,$ClO_4$-m) samples (Fig. S2), and peaks attributed to rutile were more intense and narrower than those of the starting material in spite of the presence of $ClO_4^-$, which sometimes produces the anatase phase under hydrothermal treatment from $TiCl_3$ solution (the details are discussed in section 3.4).

Figure 3 shows TEM images of the H($ClO_4$-m)S(Cl-n,$ClO_4$-0) samples. The H($ClO_4$-m)S(Cl-n,$ClO_4$-0) samples contain smaller rods than the HCn samples; however, no appreciable influence of $ClO_4^-$ concentration was observed for the H($ClO_4$-0.5)S(Cl-n,$ClO_4$-0) and H($ClO_4$-3)S(Cl-n,$ClO_4$-0) samples. These rod length and width are consistent with the $S_{BET}$ values (Table 1). This indicates that using $ClO_4^-$ ions in hydrothermal conditions retards sintering and further growth of rutile $TiO_2$ rods (the details are discussed in section 3.4).

3.4. One-step hydrothermal synthesis

$TiO_2$ was prepared by one-step hydrothermal synthesis from $TiCl_3$ solution in the presence of $ClO_4^-$ ions. Figure 4a shows an XRD pattern of the OH($ClO_4$-0.5) sample prepared using 0.5 mol $dm^{-3}$ of $NaClO_4$. The presence of $ClO_4^-$ resulted in the formation of anatase (anatase:rutile = 4:6 based on the integrated intensities of peaks attributed to anatase 101 and rutile 110[35]), although a trace of brookite was observed. The anatase phase increased with increasing $ClO_4^-$ concentration.

Figure 4b shows a TEM image of the OH($ClO_4$-0.5) sample prepared with 0.5 mol $dm^{-3}$ of $NaClO_4$. 10-nm anatase and 100-nm rutile $TiO_2$ particles (which were distinguished based on the half widths at half maximum of the XRD peaks attributed to anatase 101 and rutile 110) were observed. The large rutile particles had exposed crystal faces with aspect ratios of at most two. By contrast, $TiO_2$ obtained by hydrothermal treatment of $TiCl_3$ with 1.0 mol $dm^{-3}$ of NaCl (the OH(Cl-1) sample) consisted of rutile $TiO_2$ rods with $W_{ave}$ = 34 nm and $L_{ave}$ = 182 nm, which is a similar structure to reported rutile $TiO_2$ rods.[24] Therefore, $ClO_4^-$ ions induced both anatase formation and changed the shape of rutile $TiO_2$ particles as a result of retardation of crystal growth along the [001] direction, presumably due to the coordination of $ClO_4^-$ ions with a specific site in the nucleation process.

As mentioned in section 3.3, hydrothermal treatment of the S(Cl-n,$ClO_4$-0) sample with $ClO_4^-$ ions did not result in the formation of anatase $TiO_2$. This is because the S(Cl-n,$ClO_4$-m) samples contained almost no anatase $TiO_2$ precursors (e.g., residual $TiCl_3$ and intermediate species from $TiCl_3$) since they were almost completely hydrolyzed in the first step. Moreover, $ClO_4^-$ ions retarded sintering and crystal growth along the [001] direction and $ClO_4^-$ ions had a larger effect in the second synthesis step than in the first synthesis step. This indicates that $ClO_4^-$ ions function efficiently under hydrothermal conditions and/or in the absence of $Cl^-$ ions. Therefore, the first synthesis step is important in that anatase formation and crystal growth along the [001] direction is retarded under hydrothermal conditions in the presence of $ClO_4^-$ ions in second-step synthesis.

3.5. Correlation between crystal shape and photocatalytic activity

The photocatalytic activities of the prepared samples were evaluated using the decomposition of acetaldehyde. Figure 5 shows time courses of $CO_2$ evolution for acetaldehyde decomposition over representative $TiO_2$ under UV irradiation. Although all the samples showed similar time course curves for $CO_2$ evolution, the amount of $CO_2$ evolved varied greatly between the samples. To simplify the discussion, the amount of $CO_2$ evolved at 480 min ($M_{CO2}$) was used to estimate the photocatalytic activity.

Figure 6 shows the relationship between $S_{BET}$ and $M_{CO2}$ for the S(Cl-n,$ClO_4$-m), HS(Cl-n,$ClO_4$-m), and H($ClO_4$-m)S(Cl-n,$ClO_4$-0) samples (n and m = 0, 0.5, and 3). There is a clear correlation between $S_{BET}$ and $M_{CO2}$. $M_{CO2}$ of the HS(Cl-n,$ClO_4$-m) and H($ClO_4$-m)S(Cl-n,$ClO_4$-0) samples increased and $M_{CO2}$ of the S(Cl-n,$ClO_4$-m) samples decreased with increasing $S_{BET}$. It is difficult to discuss the relationship between $M_{CO2}$ and the particle shape of all the samples including the S(Cl-n,$ClO_4$-m) samples, whose structure differed greatly from those of the HS(Cl-n,$ClO_4$-m) and H($ClO_4$-m)S(Cl-n,$ClO_4$-0) samples. However, the increase in $M_{CO2}$ with $S_{BET}$ in the HS(Cl-n,$ClO_4$-m) and H($ClO_4$-m)S(Cl-n,$ClO_4$-0) samples can be explained by one or both of the following two hypotheses: (1) a reduction in the aspect ratio induced by an increase in $S_{BET}$, increasing the number of adsorption sites and/or (2) optimization of the surface area ratio of oxidation to reduction sites due to an increase in the number of oxidation sites.

Figure 7a shows experimentally measured $S_{BET}$ values for the HS(Cl-n,$ClO_4$-m), H($ClO_4$-m)S(Cl-n,$ClO_4$-0), and OH(Cl-1) samples together with theoretical $S_{BET}$ curves for rutile rods with {110} and {111} (dashed line) and {110} and {001} (solid line) exposed crystal faces as functions of $r_{asp}$. The theoretical $S_{BET}$ curves were calculated using a density of 4.25 g $cm^{-3}$ and a contact angle of 132.3° between the {110} and {111} planes for dodecahedral rutile. The aspect ratio was defined as the ratio of the maximum length along the [001] direction ($d_{001}$) to that along the [110] direction ($d_{110}$). The experimentally measured $S_{BET}$ agreed with the theoretical $S_{BET}$ curves calculated using $d_{110}$ = 30 nm and assuming that rutile has {110} and {001} exposed crystal faces. The reason for $d_{110}$ (30 nm) being larger than $W_{ave}$ (17–24 nm) may be because of a reduction in $S_{BET}$ due to sintering of the rutile particles.

Figure 7b shows $M_{CO2}$ and theoretical values of $S_{BET}$ as a function of the aspect ratio of the rutile rods. Some deviated plots of $M_{CO2}$ form theoretical $S_{BET}$ curves in the small $r_{asp}$ region (dotted line). This indicates that the increase in photocatalytic activity cannot be explained only by an increase in $S_{BET}$ if it is assumed that $M_{CO2}$ increases linearly with $S_{BET}$. Therefore, rutile $TiO_2$ rods with a small $r_{asp}$ are thought to exhibit higher photocatalytic activities because their surface area ratio of oxidation to reduction sites is more optimal.

## 4. Conclusions

Two-step synthesis from $TiCl_3$ solution induced formation of shape-controlled rutile rods with smaller aspect ratios ($r_{asp}$ ~ 2.0–3.2) than those of rutile rods prepared by the one-step hydrothermal method ($r_{asp}$ ~ 5.4). $Cl^-$ ions in the first step and $ClO_4^-$ ions in the second step restricted crystal growth along the [001] direction, presumably due to retardation of end-by-end attachment growth. The photocatalytic activity for decomposition of acetaldehyde increased with decreasing aspect ratio (i.e., increasing number of oxidation sites) due not to an increase in the number of adsorption sites but rather to a more optimal ratio of the surface areas of oxidation to reduction sites.

## ACKNOWLEDGMENT

This work was supported by a grant of the Knowledge Cluster Initiative implemented by the Ministry of Education, Culture, Sports, Science and Technology (MEXT).

**Supporting Information Available:** Figure S1, S2, S3, S4, S5 and S6, showing the XRD patterns and photocatalytic evaluation results of the prepared samples. This material is available free of charge via the Internet at http://pubs.acs.org.

## FIGURE CAPTIONS

**Figure 1.** TEM images of $TiO_2$ prepared by stirring of aqueous solution of $TiCl_3$ containing NaCl and $NaClO_4$ for one week. (a) S(Cl-0,$ClO_4$-0), (b) S(Cl-0,$ClO_4$-0.5), (c) S(Cl-0,$ClO_4$-3), (d) S(Cl-0.5,$ClO_4$-0), (e) S(Cl-3,$ClO_4$-0), and (f) S(Cl-3,$ClO_4$-3).

**Figure 2.** TEM images of $TiO_2$ prepared by hydrothermal treatment of S(Cl-n,$ClO_4$-m) (n and m = 0, 0.5, 3) samples. (a) HS(Cl-0,$ClO_4$-0), (b) HS(Cl-0,$ClO_4$-0.5), (c) HS(Cl-0,$ClO_4$-3), (d) HS(Cl-0.5,$ClO_4$-0), (e) HS(Cl-3,$ClO_4$-0), and (f) HS(Cl-3,$ClO_4$-3).

**Figure 3.** TEM images of $TiO_2$ prepared by hydrothermal treatment of S(Cl-n,$ClO_4$-0) (n = 0.5, 3) samples in the presence of $NaClO_4$. (a) H($ClO_4$-0.5)S(Cl-0.5,$ClO_4$-0), (b) H($ClO_4$-3)S(Cl-0.5,$ClO_4$-0), (c) H($ClO_4$-0.5)S(Cl-3,$ClO_4$-0), and (d) H($ClO_4$-3)S(Cl-3,$ClO_4$-0).

**Figure 4.** (a) XRD pattern and (b) TEM image of OH($ClO_4$-0.5).

**Figure 5.** Time courses of $CO_2$ evolution for acetaldehyde decomposition over representative $TiO_2$ samples. (a) S(Cl-3,$ClO_4$-0), (b) HS(Cl-3,$ClO_4$-0), and (c) H($ClO_4$-0.5)S(Cl-3,$ClO_4$-0).

**Figure 6.** Relationship between $S_{BET}$ and $M_{CO2}$ of S(Cl-n,$ClO_4$-m) (▲), HS(Cl-n,$ClO_4$-m) (○), and H($ClO_4$-m)S(Cl-n,$ClO_4$-0) (□) samples.

**Figure 7.** (a) Experimental $S_{BET}$ of HS(Cl-n,$ClO_4$-m) (○), H($ClO_4$-m)S(Cl-n,$ClO_4$-0) (□), and OH(Cl-1) (■) samples, and theoretical $S_{BET}$ curves for rutile $TiO_2$ rods with {110} and {111} (dashed line) and {110} and {001} (solid line) exposed crystal faces as a function of $r_{asp}$. (b) Theoretical $S_{BET}$ curve (solid lines) and $M_{CO2}$ of HS(Cl-n,$ClO_4$-m) (○), H($ClO_4$-m)S(Cl-n,$ClO_4$-0) (□), and OH(Cl-1) (■) samples as a function of $r_{asp}$.

**SCHEME TITLES**

**Scheme 1.** Dependence of aspect ratio of shape-controlled rutile rods on surface area ratio of oxidation to reduction sites, which possibly affects the photocatalytic properties.

**TABLES**

**Table 1.** Structural properties and $S_{BET}$ of rod-like particles prepared by hydrothermal treatment with and without additives.

| name | synthesis types | starting materials | $S_{BET}$ /$m^2$ $g^{-1}$ | $r_{asp}$ | $L_{ave}$ /nm | $\sigma_L$ /nm | $W_{ave}$ /nm | $\sigma_W$ /nm | $M_{CO2}$ /ppm |
|---|---|---|---|---|---|---|---|---|---|
| S(Cl-0,$ClO_4$-0) | first-step | $TiCl_3$ | 174 | – | – | – | – | – | 446 |
| S(Cl-0.5,$ClO_4$-0) | first-step | $TiCl_3$ + 0.5 mol $dm^{-3}$ of NaCl | 128 | – | – | – | – | – | 582 |
| S(Cl-3,$ClO_4$-0) | first-step | $TiCl_3$ + 3.0 mol $dm^{-3}$ of NaCl | 129 | – | – | – | – | – | 633 |
| S(Cl-0,$ClO_4$-0.5) | first-step | $TiCl_3$ + 0.5 mol $dm^{-3}$ of $NaClO_4$ | 162 | – | – | – | – | – | 598 |
| S(Cl-0,$ClO_4$-3) | first-step | $TiCl_3$ + 3.0 mol $dm^{-3}$ of $NaClO_4$ | 109 | – | – | – | – | – | 758 |
| S(Cl-3,$ClO_4$-3) | first-step | $TiCl_3$ + 3.0 mol $dm^{-3}$ of NaCl and $NaClO_4$ | 276 | – | – | – | – | – | 267 |
| HS(Cl-0,$ClO_4$-0) | second-step | S(Cl-0,$ClO_4$-0) | 46 | 3.1 | 71 | 33 | 23 | 6 | 501 |
| HS(Cl-0.5,$ClO_4$-0) | second-step | S(Cl-0.5,$ClO_4$-0) | 54 | 2.4 | 55 | 23 | 23 | 6 | 386 |
| HS(Cl-3,$ClO_4$-0) | second-step | S(Cl-3,$ClO_4$-0) | 45 | 2.5 | 58 | 21 | 23 | 7 | 383 |
| HS(Cl-0,$ClO_4$-0.5) | second-step | S(Cl-0,$ClO_4$-0.5) | 37 | 3.2 | 74 | 38 | 24 | 7 | 405 |
| HS(Cl-0,$ClO_4$-3) | second-step | S(Cl-0,$ClO_4$-3) | 46 | 2.3 | 45 | 22 | 20 | 5 | 382 |
| HS(Cl-3,$ClO_4$-3) | second-step | S(Cl-3,$ClO_4$-3) | 56 | 2.0 | 37 | 15 | 18 | 4 | 578 |
| H($ClO_4$-0.5)S(Cl-0.5,$ClO_4$-0) | second-step | HS(Cl-0.5,$ClO_4$-0) + 0.5 mol $dm^{-3}$ of $NaClO_4$ | 45 | 2.7 | 51 | 24 | 19 | 5 | 412 |
| H($ClO_4$-3)S(Cl-0.5,$ClO_4$-0) | second-step | HS(Cl-0.5,$ClO_4$-0) + 3.0 mol $dm^{-3}$ of $NaClO_4$ | 42 | 2.8 | 60 | 25 | 21 | 6 | 527 |
| H($ClO_4$-0.5)S(Cl-3,$ClO_4$-0) | second-step | HS(Cl-3,$ClO_4$-0) + 0.5 mol $dm^{-3}$ of $NaClO_4$ | 63 | 2.0 | 34 | 14 | 17 | 4 | 798 |
| H($ClO_4$-3)S(Cl-3,$ClO_4$-0) | second-step | HS(Cl-3,$ClO_4$-0) + 3.0 mol $dm^{-3}$ of $NaClO_4$ | 61 | 2.0 | 37 | 15 | 19 | 4 | 537 |
| OH(Cl-1) | single-pot | $TiCl_3$ + 1.0 mol $dm^{-3}$ of NaCl | 21 | 5.4 | 182 | 88 | 34 | 14 | 377 |
| OH($ClO_4$-0.5) | single-pot | $TiCl_3$ + 0.5 mol $dm^{-3}$ of $NaClO_4$ | – | – | – | – | – | – | – |

**REFERENCES**


(1) Fujishima, A.; Rao, T. N.; Tryk, D. A. *J. Photochem. Photobiol. C: Photochem. Reviews* **2000**, *1*, 1.

(2) Hoffmann, M. R.; Martin, S. T.; Choi, W.; Bahnemann, D. W. *Chem. Rev.* **1995**, *95*, 69.

(3) Maeda, K.; Domen, K. *J. Phys. Chem. C* **2007**, *111*, 7851.

(4) Osterloh, F.E. *Chem. Mater.* **2008**, *20*, 35.

(5) Maeda, K.; Domen, K. *Chem. Mater.* **2010**, *22*, 612.

(6) Roy, S. C.; Varghese, O. K.; Paulose, M.; Grimes, C. A. *ACS NANO* **2010**, *4*, 1259.

(7) Mahaney, O.O.P.; Murakami, N.; Abe, R.; Ohtani, B. *Chem. Lett.* **2009**, *38*, 238.

(8) Ohno, T.; Sarukawa, K.; Matsumura, M. *New. J. Chem.* **2002**, *26*, 1167.

(9) Yoshinaga, K.; Yamauchi, M.; Maruyama, D.; Mouri, E.; Koyanagi, T. *Chem. Lett.* **2005**, *34*, 1094.

(10) Hosono, E.; Fujihara, S.; Kakiuchi, K.; Imai, K. *J. Am. Chem. Soc.* **2004**, *126*, 7790.

(11) Kakiuchi, K.; Hosono, E.; Imai, H.; Kimura, T.; Fujihara, S. *J. Cryst. Growth* **2006**, *293*, 541.

(12) Wang, D.; Liu, J.; Huo, Q.; Nie, Z.; Lu, W.; Williford, R. E.; Jiang, Y. *J. Am. Chem. Soc.* **2006**, 128, 13670.

(13) Amano, F.; Yasumoto, T.; Mahaney, O.O.P.; Uchida, S.; Shibayama, T.; Ohtani, B. *Chem. Comm.* **2009**, 2311.

(14) Zhang, D.; Li, G.; Wang, H.; Chan, K.M.; Yu, J.C. *Crystal Growth & Design* **2010**, *10*, 1130.

(15) Dai, Y.; Cobley, C. M.; Zeng, J.; Sun, Y.; Xia, Y. *Nano Lett.* **2009**, *9*, 6.

(16) Amano, F.; Mahaney, O.O.P.; Terada, Y.; Yasumoto, T.; Shibayama T.; Ohtani, B. *Chem. Mater.* **2009**, 21, 2601.

(17) Li, J.; Xu, D. *Chem. Commun.* **2010**, *46*, 2301.

(18) Li, J.; Yu, Y.; Chen, Q.; Li, J.; Xu, D. *Cryst. Growth Des.* **2010**, *10*, 2111.

(19) Li, Y.; Lee, N.; Hwang, D.; Song, J. S.; Lee, E. G.; Kim, S. *Langmuir* **2004**, *20*, 10838.

(20) Yang, H. G.; Sun, C. H.; Qiao, S. Z.; Zou, J.; Liu, G. ; Smith, S. C.; Cheng H. M.; Lu, G. Q. *Nature* **2008**, *453*, 638.

(21) Yang, H. G.; Liu, G.; Qiao, S. Z.; Sun, C. H.; Jin, Y. G.; Smith, S. C.; Zou, J.; Cheng, H. M.; Lu, G. Q. *J. Am. Chem. Soc.* **2009**, *131*, 4078.

(22) Zhu, J.; Wang, S.; Bian, Z.; Xie, S.; Cai, C.; Wang, J.; Yang, H.; Li, H. *CrystEngComm* **2010**, *12*, 2219.

(23) Amano, F.; Yasumoto, T.; Mahaney, O.O.P.; Uchida, S.; Shibayama, T. *Top. Catal.* **2010**, *53*, 455.

(24) Bae, E.; Murakami, N.; Ohno, T. *J. Molec. Catal. A: Chem.* **2009**, *300*, 72.

(25) Bae, E.; Ohno, T. *Appl. Catal. B: Environ.* **2009**, *91*, 634.

(26) Bae, E.; Murakami, N.; Nakamura, M.; Ohno, T. *Appl. Catal. A: Gen.* **2010**, *380*, 48.

(27) Murakami, N.; Kurihara, Y.; Tsubota, T.; Ohno, T. *J. Phys. Chem. C* **2009**, *113*, 3062.

(28) Oliver, P. M.; Watson, G. W.; Kelsey, E. T.; Parker, S. C. *J. Mater. Chem.* **1997**, *7*, 563.

(29) Barnard, A.S.; Zapol, P. *J. Phys. Chem. B* **2004**, *108*, 18435.

(30) Barnard, A. S.; Curtiss, L. A. *Nano Lett.* **2005**, *5*, 1261.

(31) Yin, H.; Wada, Y.; Kitamura, T.; Kambe, S.; Murasawa, S.; Mori, H.; Sakata, T.; Yanagida, S. *J. Mater. Chem.* **2001**, *11*, 1694.

(32) Li, Y.; Fan, Y.; Chena, Y. *J. Mater. Chem.* **2002**, *12*, 1387.

(33) Zhang, Q.; Gao, L. *Langmuir* **2003**, *19*, 967.

(34) Pottier, A.; Chanéac, C.; Tronc, E.; Mazerolles L.; Jolivet, J. *J. Mater. Chem.* **2001**, *11*, 1116.

(35) Zang, H.; Banfield, J. *J. Phys. Chem. B* **2000**, *104*, 3481.

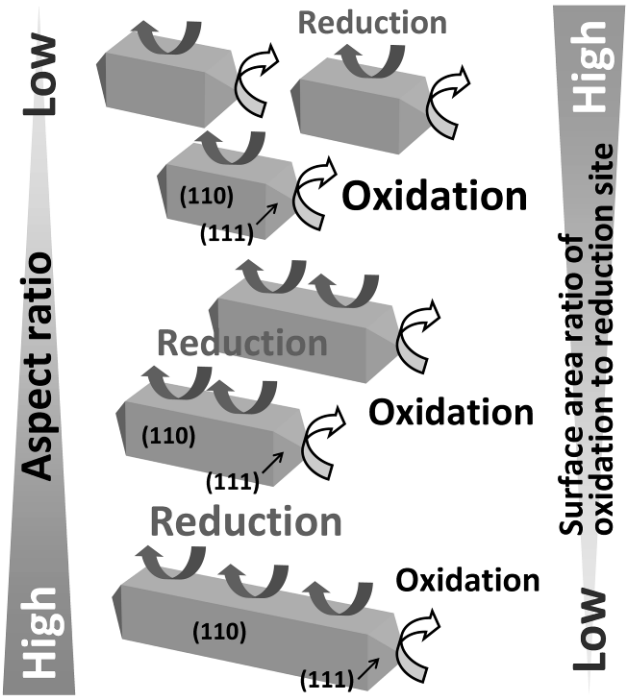


**Scheme 1.** Dependence of aspect ratio of shape-controlled rutile rods on surface area ratio of oxidation to reduction sites, which possibly affects the photocatalytic properties.

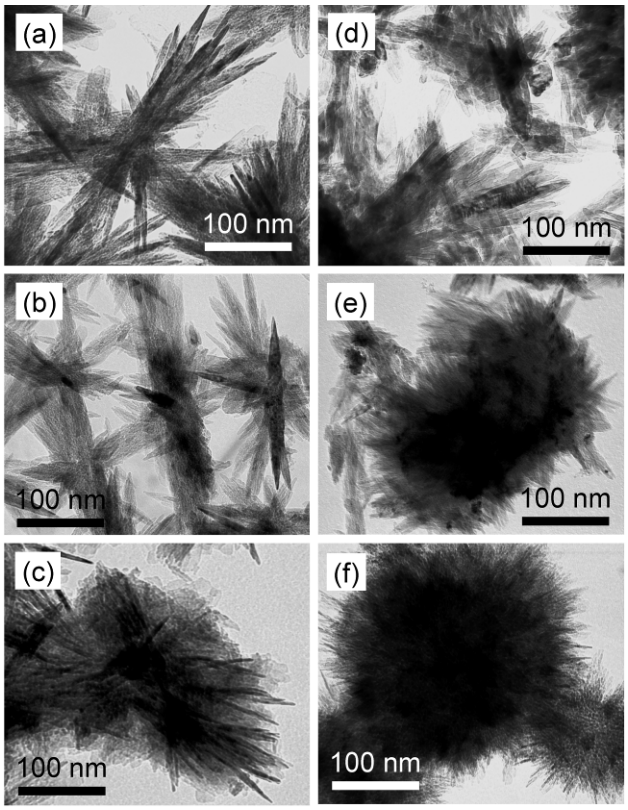


**Figure 1.** TEM images of $TiO_2$ prepared by stirring of aqueous solution of $TiCl_3$ containing NaCl and $NaClO_4$ for one week. (a) S(Cl-0,$ClO_4$-0), (b) S(Cl-0,$ClO_4$-0.5), (c) S(Cl-0,$ClO_4$-3), (d) S(Cl-0.5,$ClO_4$-0), (e) S(Cl-3,$ClO_4$-0), and (f) S(Cl-3,$ClO_4$-3).

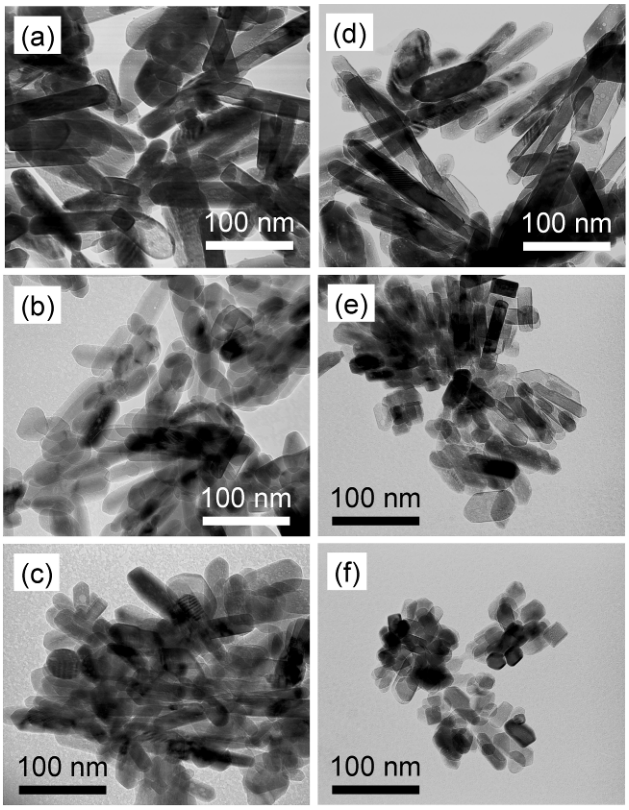


**Figure 2.** TEM images of $TiO_2$ prepared by hydrothermal treatment of S(Cl-n,$ClO_4$-m) (n and m = 0, 0.5, 3) samples. (a) HS(Cl-0,$ClO_4$-0), (b) HS(Cl-0,$ClO_4$-0.5), (c) HS(Cl-0,$ClO_4$-3), (d) HS(Cl-0.5,$ClO_4$-0), (e) HS(Cl-3,$ClO_4$-0), and (f) HS(Cl-3,$ClO_4$-3).

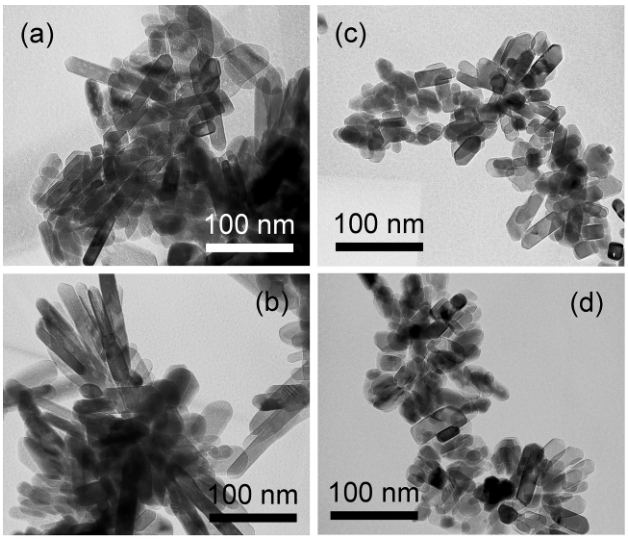


**Figure 3.** TEM images of $TiO_2$ prepared by hydrothermal treatment of S(Cl-n,$ClO_4$-0) (n = 0.5, 3) samples in the presence of $NaClO_4$. (a) H($ClO_4$-0.5)S(Cl-0.5,$ClO_4$-0), (b) H($ClO_4$-3)S(Cl-0.5,$ClO_4$-0), (c) H($ClO_4$-0.5)S(Cl-3,$ClO_4$-0), and (d) H($ClO_4$-3)S(Cl-3,$ClO_4$-0).

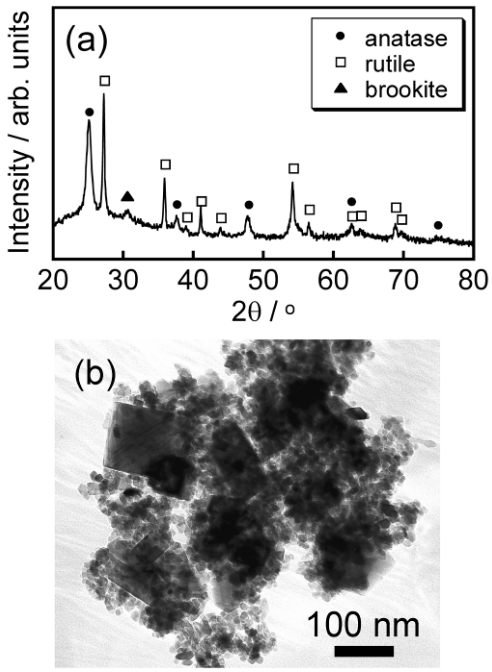


**Figure 4.** (a) XRD pattern and (b) TEM image of OH($ClO_4$-0.5).

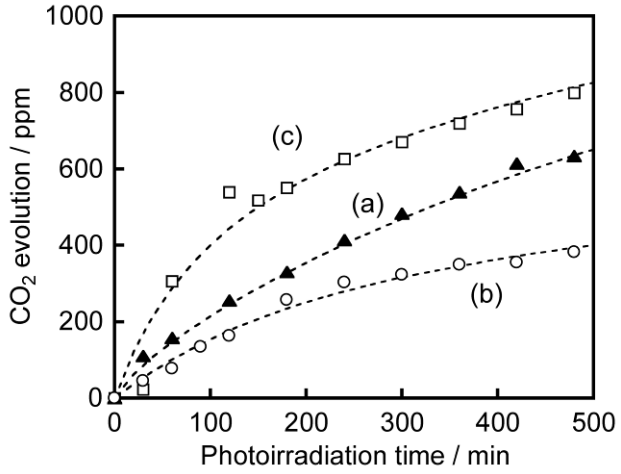


**Figure 5.** Time courses of $CO_2$ evolution for acetaldehyde decomposition over representative $TiO_2$ samples. (a) S(Cl-3,$ClO_4$-0), (b) HS(Cl-3,$ClO_4$-0), and (c) H($ClO_4$-0.5)S(Cl-3,$ClO_4$-0).

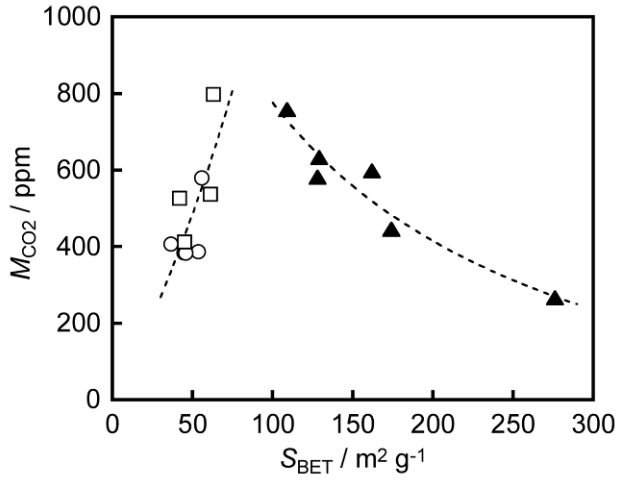


**Figure 6.** Relationship between $S_{BET}$ and $M_{CO2}$ of S(Cl-n,$ClO_4$-m) (▲), HS(Cl-n,$ClO_4$-m) (○), and H($ClO_4$-m)S(Cl-n,$ClO_4$-0) (□) samples.

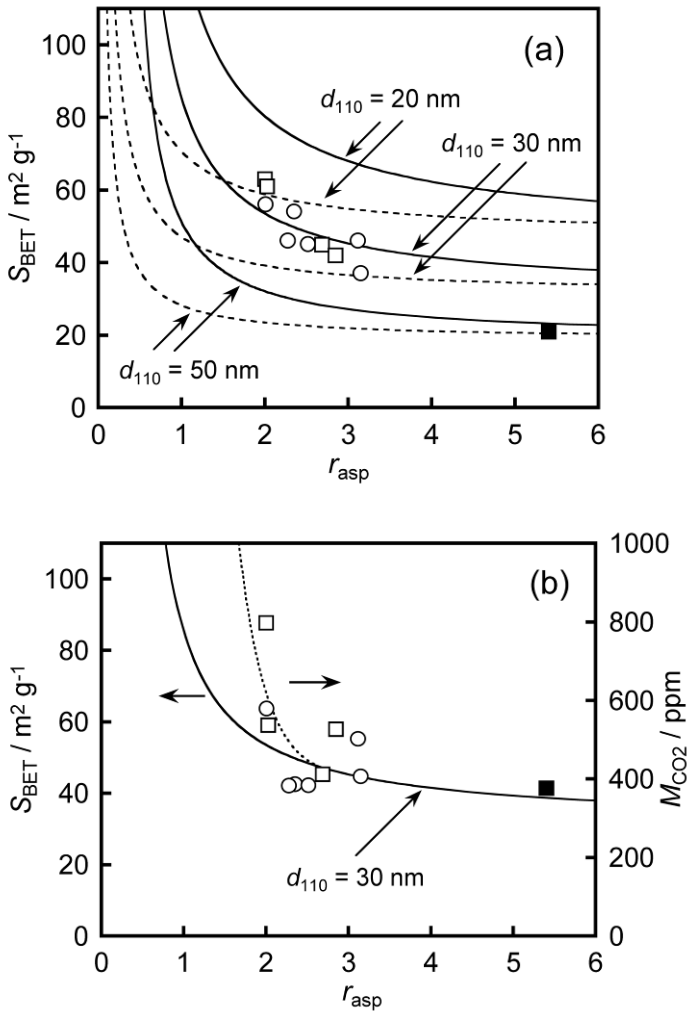


**Figure 7.** (a) Experimental $S_{BET}$ of HS(Cl-n,$ClO_4$-m) (○), H($ClO_4$-m)S(Cl-n,$ClO_4$-0) (□), and OH(Cl-1) (■) samples, and theoretical $S_{BET}$ curves for rutile $TiO_2$ rods with {110} and {111} (dashed line) and {110} and {001} (solid line) exposed crystal faces as a function of $r_{asp}$. (b) Theoretical $S_{BET}$ curve (solid lines) and $M_{CO2}$ of HS(Cl-n,$ClO_4$-m) (○), H($ClO_4$-m)S(Cl-n,$ClO_4$-0) (□), and OH(Cl-1) (■) samples as a function of $r_{asp}$.